Quaternary International 449 (2017) 1–11

Contents lists available at ScienceDirect

Quaternary International

journal homepage: www.elsevier.com/locate/quaint

A high-resolution hydrogen isotope record of behenic acid for the past 16 kyr in the northeastern United States

Li Gao [a, 1], Yongsong Huang [a, *], Bryan Shuman [b], W. Wyatt Oswald [c], David Foster [d]

[a] Department of Geological Sciences, Brown University, Providence, RI, 02912, USA
[b] Department of Geology and Geophysics, University of Wyoming, Laramie, WY, 82071, USA
[c] Emerson College, 120 Boylston Street, Boston, MA, 02116, USA
[d] Harvard Forest, Harvard University, Petersham, MA, 01366, USA

ARTICLE INFO

Article history:
Received 19 October 2016
Received in revised form
23 April 2017
Accepted 21 June 2017
Available online 3 July 2017

Keywords:
Hydrogen isotopes
Leaf lipids
Precipitation-weighted temperature
Drought
Holocene climate
New England
Northeastern USA

ABSTRACT

D/H ratios of leaf lipids from lacustrine aquatic macrophytes have been shown to record precipitation δD values, which can reflect precipitation-weighted mean annual temperature (MAT) in the northeastern United States. Here we report a high-resolution hydrogen isotopic record from Little Pond, Massachusetts, USA, which we compare with other paleoclimate data from the region, including a similar δD record from Blood Pond, Massachusetts. Together the two datasets provide a >16 ka record of δD variability in the region, affording new insights into Holocene climate history. First, the long-term trends in δD correlate significantly with regional temperatures inferred from alkenone records from nearby areas of the North Atlantic and lake-level inferred changes in precipitation and evaporation. The long-term δD trends reflect a period of maximum regional warmth at ca. 8–6 ka after the collapse of the Laurentide Ice Sheet. Second, unlike the positive relationship between temperature and δD observed over the long-term and during early events like the Younger Dryas, we find that a series of warm and dry events at 4.9–4.6, 4.2–3.9, 2.9–2.1, and 1.3–1.2 cal kya BP coincide with negative δD excursions from the long trends. These events were likely driven by summer drought dynamics.

1. Introduction

Paleoclimate reconstructions from New England in the northeastern United States provide major reference for evaluating modern climate change and climate forcings. Such efforts include pollen (e.g., Webb et al., 2003; Shuman et al., 2007; Oswald et al., 2010; Williams et al., 2010; Marsicek et al., 2013), chironomid assemblages (Cwynar and Spear, 2001; Francis and Foster, 2001), alkenone ratios (Sachs, 2007), lithological characteristics (Shuman et al., 2001; Newby et al., 2009; Hubeny et al., 2011) and organic biomarker hydrogen isotopes (e.g., Huang et al., 2002; Shuman et al., 2006; Hou et al., 2007, 2012). These records reveal rich information on past precipitation and temperature at different time scales, including both long-term climate trends and multi-century variability. For example, early-Holocene warming led to peak temperatures during ca. 9000-5500 cal yr BP and was followed by subsequent long-term cooling (Marsicek et al., 2013; Sachs, 2007; Shuman and Marsicek, 2016). Effective moisture increased as the temperatures declined (Marsicek et al., 2013; Newby et al., 2014; Shuman and Marsicek, 2016), and a series of multi-century cool-wet/warm-dry fluctuations punctuated the long trends since ca. 6 ka (Sachs, 2007; Newby et al., 2014; Shuman and Marsicek, 2016).

Major paleoclimate questions remain, particularly about the patterns and causes of the multi-century climate variability (Newby et al., 2014; Shuman and Marsicek, 2016). Although stable isotope records from ice cores and speleothems can provide detailed paleoclimate records on time scales from decades to millennia (e.g., Grootes and Stuiver, 1997; Wang et al., 2004, 2008; Vinther et al., 2009), New England is devoid of such paleoclimate archives. In the recent years, hydrogen isotope records from sedimentary lipids have shown major advantage in recording high resolution temperature and precipitation regime changes in this region (Huang et al., 2002; Shuman et al., 2006; Hou et al., 2007, 2012). When compared with multiple, quantitative climate signals from pollen, alkenones, and lake-level studies (Sachs, 2007; Newby et al., 2014;

* Corresponding author.
E-mail addresses: li.gao@peeri.org (L. Gao), Yongsong_huang@brown.edu (Y. Huang).
[1] Present address: Power Environmental Energy Research Institute, Covina, CA 91722, USA.

http://dx.doi.org/10.1016/j.quaint.2017.06.053
1040-6182/

Shuman and Marsicek, 2016), the integrated paleoclimate data would provide an important framework for considering the influences of different climate forcings, such as orbitally-forced insolation trends (e.g., Shuman and Donnelly, 2006), the Laurentide Ice Sheet (Shuman et al., 2006; Hou et al., 2007, 2012), and solar activity (e.g, Nichols and Huang, 2012).

Recent studies demonstrate that δD values of mid-chain length leaf lipids (e.g., behenic acid δD (δD_{BA})) from aquatic macrophytes preserved in lake sediments are useful proxies for lake water δD values (Hou et al., 2006, 2007), and can therefore capture the different isotopic signatures integrated by the lake water. Lakes with abundant aquatic plant inputs are particularly attractive, because terrestrial plants also produce small amounts of mid-chain leaf waxes and could potentially interfere with aquatic plant isotopic signals (Gao et al., 2011). To deal with this problem, Gao et al. (2011) developed a model for selecting the most suitable lakes for hydrogen isotopic reconstruction (see Methods section for more details). We produce a new high-resolution, Holocene-length, behenic acid δD (δD_{BA}) record from Little Pond, located in the town of Royalston, central Massachusetts, USA. Then, using existing data from Blood Pond, also located in central Massachusetts (Hou et al., 2006, 2007), we produce a composite isotopic record in New England for the past 16 kyr.

To understand the climate signals embedded in the Little Pond δD_{BA} record, we statistically decomposed the time series and compared both the raw data series and the different spectral components with two regional datasets: an ensemble of multiple quantitative precipitation minus evaporation (P-E) reconstructions based on lake-level records from eastern Massachusetts (Newby et al., 2014; Shuman and Marsicek, 2016), and the nearest Holocene-length alkenone-derived sea-surface temperature (SST) record from the Scotian margin (Sachs, 2007). The P-E and SST records are significantly correlated at centennial scales with each other and with pollen-inferred precipitation and temperature reconstructions, and thus represent well-validated climate signals for the region (Marsicek et al., 2013; Shuman and Marsicek, 2016). Using these datasets, we evaluate 1) how the isotopic variations correspond to the temperature and moisture variations, and 2) how the variations relate to the different climate forcings in this region at different time scales. Thus, the comparisons presented here further test and expand a multifaceted framework for understanding the climate history of the North Atlantic region as expressed in New England, and reveal different interacting temperature and moisture dynamics at multi-millennial and multi-century scales.

2. Samples and methodology

2.1. Samples, study sites and chronology

For the Holocene temperature reconstruction, we collected a sediment core from Little Pond in Royalston, Massachusetts, USA (referred to as Little Pond Royalston in Oswald et al., 2007) (Fig. 1). Little Pond (42.68°N, 72.19°W, Elevation 301 m) is a small water body, that has a surface area of 4.0 ha and a maximum depth of 5.7 m. In Royalston, the long-term mean January temperature ranges from −12.3 to −0.2 °C, and the long-term July mean temperature from 13.5 to 27.7 °C (https://www.ncdc.noaa.gov/cdo-web/search; 1949–2015). Annual mean precipitation is ~1108 mm. The long-term mean January and July precipitation rates are ~85 mm/month and ~117 mm/month respectively (same source as temperatures). Little Pond is characterized by high aquatic productivity and abundant aquatic vegetation; the surrounding landscape is mainly forested. The watershed contour of Little Pond is provided in Supplementary Material (Fig. S1). The pond has one inlet and one outlet with an estimate of residence time of months to a few years based on previous study on New England lakes (Norton et al., 1989).

Modern moisture sources of our study site are estimated in Fig. S2A, based on detailed data from a recent publication by Puntsag et al. (2016). Basically, there are four principal sources of moisture for our study area, namely, south Atlantic, Northeastern Atlantic, Arctic, and western continental sources. These sources have mean δD values shown in Supplementary Table S1 and Fig. S2B. The study site reported in Puntsag et al. is at Hubbard Brook Experimental Forest, ~130 miles north of our site. We use the long-term isotopic data from Hubbard Brook Experimental Forest to approximate our isotopic values, by making a correction based on the modern offset between LPR and Hubbard Brook using the Online Isotopes in Precipitation Calculator (OIPC). Hysplit data in 2016 are also plotted to corroborate the moisture sources (Fig. S2C; Stein et al., 2015; Rolph, 2017).

The sediment core from Little Pond was collected in 2003, with a total length of ~7.8 m. The Little Pond age-depth model (Fig. S3) was generated using Bchron (Haslett and Parnell, 2008) and based on the chronological data reported by Oswald et al. (2007) (seven AMS 14C dates and pollen evidence for European settlement) plus an additional ^{14}C date obtained for the depth of 712–713 cm (OS-82883; ^{14}C age = 9940 ± 45). The resulting sampling resolution was ~40 yr between 11 and 8 cal kyr BP, and ~80 yr between 8 cal kyr BP and present (about 10 yr resolution in the past 200 yr).

We statistically compared the details of the Little Pond record with the average P-E reconstruction from New Long Pond in Plymouth, Massachusetts (150 km SE of Little Pond), and Deep Pond in Falmouth, Massachusetts (175 km SE of Little Pond; Marsicek et al., 2013; Newby et al., 2014), and with the Uk'37 SST reconstruction from core OCE326-GGC30 from off the coast of Nova Scotia (Sachs, 2007), which was not significantly different, including its centennial details, from pollen-inferred growing-season temperatures from the region from Maine to New York (Shuman and Marsicek, 2016). Consistent with previous analyses, the SST record was linearly detrended to account for a warm-bias that causes Late-Pleistocene temperatures to be > 5 °C warmer than today in the raw data (see discussion by Shuman and Marsicek, 2016).

We also made a composite δD_{BA} record using our new data from Little Pond and the published δD_{BA} data from Blood Pond, south Massachusetts (Hou et al., 2007), which is ~80 km south of Little Pond, has a surface area of 8.5 ha, and reaches a maximum depth of 3.6 m. In Dudley, Massachusetts, where Blood Pond is located, the long-term mean January temperature ranges from −9.8 to 0.7 °C, and the long-term July mean temperature from 15.5 to 27.0 °C (source: http://www.ncdc.noaa.gov/cdo-web/;monthly normals for Charlton, MA; 1951–2016). Annual mean precipitation is ~1220 mm, which is evenly distributed throughout the year (same source as temperature). Temperatures are slightly warmer at Blood Pond than near Little Pond by around 1.9, 1.2, and 1.3 °C for the average high and low temperatures in January and the average low temperatures in July, respectively.

The existing Blood Pond δD_{BA} record (Hou et al., 2006, 2007, 2012) features about 90 yr resolution between 16 and 10 cal kyr BP and about 20 yr resolution from 10 cal kyr BP to 7.5 cal kyr BP (Fig. S3). To make the composite record from these two cores, we have aligned the Blood Pond record to the Little Pond record and reduced the Blood Pond δD_{BA} values by 5‰ in order to account for the slightly warmer temperature at that site. The δD of modern lake water from Blood Pond is also ~5‰ higher than that from Little Pond (Fig. 2A), which may reflect the slightly higher temperature, and/or different proportion of plant input sources (Gao et al., 2011). Applying such a small offset correction led to visually more consistent overlapping of the two records for the time interval of

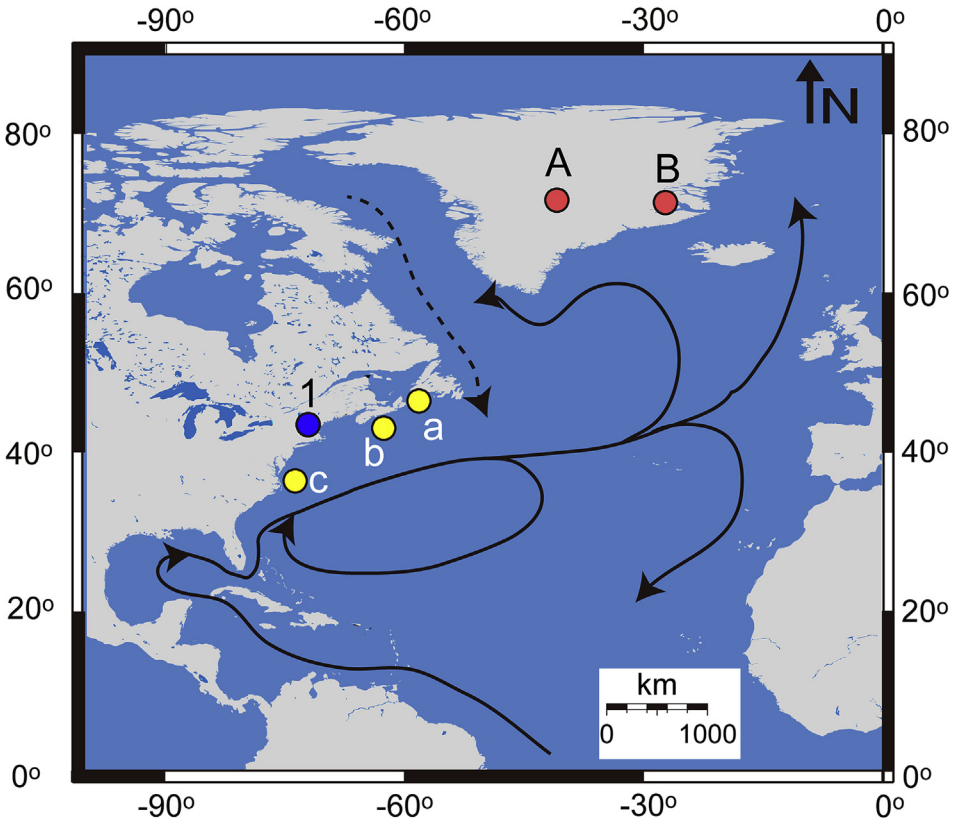

Fig. 1. Map of the study sites and geographical settings. The solid black lines depict the Gulf Stream and the dashed line indicates the Labrador Current. The study sites are 1) Little Pond (this study; Marsicek et al., 2013) and Blood Pond (Hou et al., 2007, 2012; Marsicek et al., 2013). a-c) the alkenone-based SSTs in northwestern N. Atlantic (b is the Scotian Margin site; Sachs, 2007), A) GISP2 $\delta^{18}O$ (Grootes and Stuiver, 1997) and B) Renland $\delta^{18}O$ (Vinther et al., 2009). The Rocky Pond with % Coarse material and Crooked Pond with lake level reconstruction are close to the position (1) (Newby et al., 2009; Shuman et al., 2001). Regionally-synthesized pollen-inferred temperatures are also available from the northeastern US (Shuman et al., 2007; Marsicek et al., 2013), and N. Quebec (Viau et al., 2006).

11.3–8 ka, during which both lakes have high-resolution δD data.

To test for a significant evaporative enrichment of deuterium in the modern lake waters, surface lake water δD and $\delta^{18}O$ values for both lakes were measured in August 2009 (Fig. 2A). The δD and $\delta^{18}O$ values were compared with the local meteoric water line, which is established based on precipitation δD and $\delta^{18}O$ data from the Global Network of Isotopes in Precipitation (GNIP) stations in New England (IAEA, 2006). There were 745 usable data points from 7 GNIP stations in the eastern North America (Supplementary Table S2) and the data coverage was from 1953 to 2007.

To evaluate how temperature changes influence the downcore δD_{BA} values, we compare the δD_{BA}-reconstructed temperatures from Little Pond (about 10 yr resolution for the past 200 yrs) with the 180-year instrumental record of mean annual temperature for Amherst, Massachusetts (Fig. 2B; Amherst temperature sources: the full record (1836–2015) was made by Prof. R Bradley and M. Rawlins, including the averaged overlap between data from the National Climatic Data Center, National Oceanic and Atmospheric Administration (http://www.ncdc.noaa.gov/cdo-web/) and the book by Bradley et al. (1987). In Amherst, Massachusetts, the long-term mean January temperature ranges from −10.4 to 0.6 °C, and the long-term July mean temperature from 15.1 to 27.9 °C (source: http://www.ncdc.noaa.gov/cdo-web/; monthly normals for Amherst, MA). Annual mean precipitation is ~1169 mm, which is relatively evenly distributed throughout the year (same source as temperature).

To best reconstruct source water hydrogen isotopic ratios using compound-specific isotope analysis, we must also determine the source of the target compound(s) because different sources may carry distinct isotope signatures and blur the climate change-induced isotope variations. We have thus assessed the aquatic inputs of mid-chain leaf lipids in Little Pond and Blood Pond using the multi-source mixing model developed by Gao et al. (2011). Briefly, the *n*-alkane distributions of different groups of plants (e.g., submerged/floating, terrestrial, etc) are used as end members in a linear algebra model. The sedimentary *n*-alkane distributions from study lakes are thus considered mixture from different end members. The best fit of each end-member inputs to sediments is thus optimized in Matlab Software.

2.2. Analytical method

The sediment samples were prepared and analyzed following the procedure in Gao et al. (2011). All sediment samples were first freeze-dried. The samples (~0.2 g dw) were extracted using an Accelerated Solvent Extractor (ASE200, Dionex) with dichloromethane:methanol (9:1 v/v) at 150 °C and 1200 psi for three 15-min cycles. The total extracts were then separated into neutral and acid fractions using solid phase extraction (Aminopropyl Bond Elute ®). The acid fractions were methylated overnight using 5% acetyl chloride in methanol at 60 °C. Methylated acids were recovered after addition of ~3 ml 5% NaCl water solution and extracted with hexane. Hydroxyl acids were removed using silica gel column chromatography. The fatty acid methyl esters (FAMEs) were collected in dichloromethane. The neutral fraction was further eluted through silica gel columns with hexane, dichloromethane, 25% ethyl acetate in hexane and methanol to get hydrocarbon, ketone/ester/aromatic fractions, alcohols and others, consecutively.

To determine the *n*-alkyl lipid distributions, FAMEs and

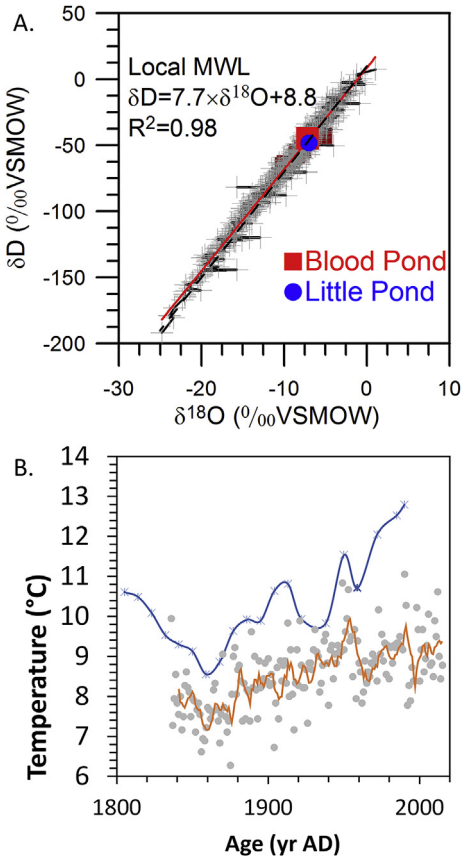

Fig. 2. A) Comparison of the lake water δD and $\delta^{18}O$ values of Little Pond and Blood Pond with the local Meteoric Water Line (MWL); B) Comparison of the δD_{BA}-inferred temperature (gray * symbols and the blue line) from Little Pond with instrumental records from nearby City of Amherst (gray dots for the original yearly data and the orange line for 5-yr running average). The local MWL is established based on precipitation δD and $\delta^{18}O$ data from Global Network of Isotopes in Precipitation (GNIP) stations in New England (IAEA, 2006). Global MWL is also plotted (the dashed line). Surface lake water from Blood Pond and Little Pond was collected in August 2009. Error bars for the δD and $\delta^{18}O$ of the lake water for both lakes are smaller than the symbol size on Fig. 2A. The instrumental temperature data for Amherst City are obtained from the National Oceanographic and Atmospheric Administration's National Climatic Data Center (NCDC), NOAA. Analytical errors for δD values of behenic acid in Fig. 2B are smaller than 3‰ and not visible. (For interpretation of the references to colour in this figure legend, the reader is referred to the web version of this article.)

hydrocarbon fractions were analyzed using a gas chromatograph (GC, Agilent model 6890) with injector split/splitless and flame ionization detector (FID). Chemstation version B.03.01 software was used for data acquisition and analysis. Compound identification was based on comparison of GC retention times and mass spectra from GC-MS (Gas Chromatography-Mass Spectrometry) analyses. GC-MS analysis was carried out on an Agilent 5973N quadrupole mass analyzer interfaced to an Agilent GC model 6890N. Chemstation E. 02.00 software was used for data acquisition and analysis.

Hydrogen isotopic ratios for *n*-alkanes and *n*-alkanoic acids are measured on an HP 6890 chromatography interfaced to a Finnigan Delta + XL stable isotope mass spectrometer through a high temperature pyrolysis reactor (Huang et al., 2002, 2004; Hou et al., 2007). The H_3^+ factor was determined every two days prior to sample analysis (average values 3.0 ± 0.3 during this study). The precision (1σ) of duplicate analyses was within ±3‰. The accuracy was routinely checked by analyses of laboratory isotopic standards between every 6 samples (C_{23}, C_{27}, C_{29} *n*-alkanes; C_{22}, C_{24}, C_{28} *n*-alkanoic acids). The δD values for individual *n*-acids (as methyl esters) were corrected by mathematically removing the isotopic contributions of the added methyl group. The δD values of the added methyl group were determined by acidifying and then methylating (along with the samples) the disodium salt of succinic acid with a predetermined δD values (Huang et al., 2002).

The lake water was collected in 2 mL vial and sealed for isotopic analyses. The water samples were analyzed for δD and $\delta^{18}O$ following the same procedures as in Gao et al. (2012). The lake water samples were charcoal processed to remove organic compounds, then analyzed in a model L1102-i isotopic liquid water and water vapor analyzer (Picarro, Sunnyvale, CA, USA). The instrument was routinely checked for accuracy and precision using our secondary isotopic standards with δD values of 31, −38 and −256% VSMOW. The standard deviation was <0.1% for $\delta^{18}O$ values and <0.6% for δD values.

2.3. Statistical methods

To decompose and compare the Little Pond δD_{BA} record, the ensemble average P-E reconstruction, and the Uk'37 SST series, we fit generalized additive mixed models (GAMMs) to each time series, which enabled us to conduct high-pass filtering via detrending. GAMMs are locally fit polynomials that can account for non-linear trends and temporal autocorrelation among the residuals (Wood, 2006). The GAMMs were all fit in R (R Core Development Team, 2009) using the mgcv package. They have the form $Data_A \sim s$ (Age) where s represents a spline smoother and A equals δD_{BA}, P-E, or SST. The models include a linear mixed effects model with an ARIMA (autoregressive integrative moving average model) correlation structure based on age. To ensure that the GAMMs capture only the lowest frequency (>3000 year) trends, the smoother (s) has a basis dimension, k, equal to only 4, which sets an upper limit on the number of degrees of freedom. The order of the ARIMA correlation structure derives from the R function, ar, applied to each of the raw datasets.

Pearson product-moment correlations, r, were calculated for each pair of raw or detrended data (e.g., raw and detrended δD_{BA} versus raw and detrended P-E series). To assess the significance of the correlations, we also compared the coefficients with those generated from calculating the correlation of each dataset (e.g., δD_{BA}) with 1000 random autoregressive time series generated using the function, arima.sim, in R based on the autoregressive coefficients calculated for the actual data using the function, ar. The comparison tests whether correlation exists simply because of similar orders of autoregression (e.g., similarly smooth trends) or whether the correlations exceed the range expected from chance alone. We use histograms to compare the correlation coefficients from comparisons of the data with the 1000 random coefficients, and assess whether correlation coefficients based on the data fall outside the 95% range of random values. Linear models (using the function, lm, in R) and Granger causality tests (grangertest in R) enable us to further quantify the relationships between the climate variables and δD_{BA}.

To facilitate comparison across datasets, all data were first linearly interpolated to 50-yr intervals. Because the P-E reconstruction lacks detail in the early Holocene, we only use the last 8500 years for the detrended comparisons. We also split the data into Early- and Late-Holocene components at 6250 cal yr BP based on significant changes in correlation coefficients at that time.

3. Results

3.1. Comparison of the Little Pond δD_{BA} record with other paleoclimate records

The SST and P-E reconstructions, which we compare with the

Little Pond δD_{BA} record, indicate that temperature and moisture followed different long-term trends over the Holocene in Massachusetts (Fig. 3A). Temperatures and effective moisture both increased prior to ca. 8 ka, but since then, temperatures declined by ~2 °C as effective moisture increased by ~200 mm of equivalent precipitation (Shuman and Marsicek, 2016). SST and P-E are poorly correlated overall ($r = 0.17$), but have a negative correlation ($r = -0.41$) over the last 6250 years when both records have comparable detail. The correlation differs significantly from random expectations (inset histogram, Fig. 3A) and is expressed both in the long-term trend (Fig. 3A) and multi-century events (Fig. 3B). Together, the SST and P-E datasets capture a series of cool/wet and warm/dry multi-century fluctuations (Fig. 3B). The warm/dry episodes were statistically synchronous with ages of 4.9–4.6, 4.2–3.9, 2.9–2.1, and 1.3–1.2 cal kyr BP in multiple records (Newby et al., 2014).

Comparison of the two paleoclimate reconstructions with the Little Pond δD_{BA} record indicates that the long-term trends and multi-century events have different isotopic signatures (Figs. 4–5). The long-term trends in δD_{BA}, described by the GAMMs (Fig. 4A), positively correlate with the long-term SST trends ($r = 0.57$; Fig. 4A) and negatively correlate with the long-term P-E trends ($r = -0.68$; Fig. 5A). Based on the smooth trends of the GAMMs, δD_{BA} tended to decline as temperature declined: $\delta D_{BA\text{-}smooth} = (3.1 \pm 0.29‰/°C)\ T_{smooth} - 193.3 \pm 3.6‰$ (adjusted $R^2 = 0.31$, $p < 2.2e\text{-}16$); a Granger causality test indicates that the two smoothed series contribute more information to predicting each other than autocorrelation in each series alone ($F > 370$, $p < 2.2e\text{-}16$). At the same time, δD_{BA} also tended to decline as effective moisture increased, which could be consistent with evaporative effects: $\delta D_{BA\text{-}smooth} = (-0.024 \pm 0.002‰/mm)\ P\text{-}E_{smooth} - 0.016 \pm 3.6‰$ (adjusted $R^2 = 0.45$, $p < 2.2e\text{-}16$); Granger causality was also detected in this

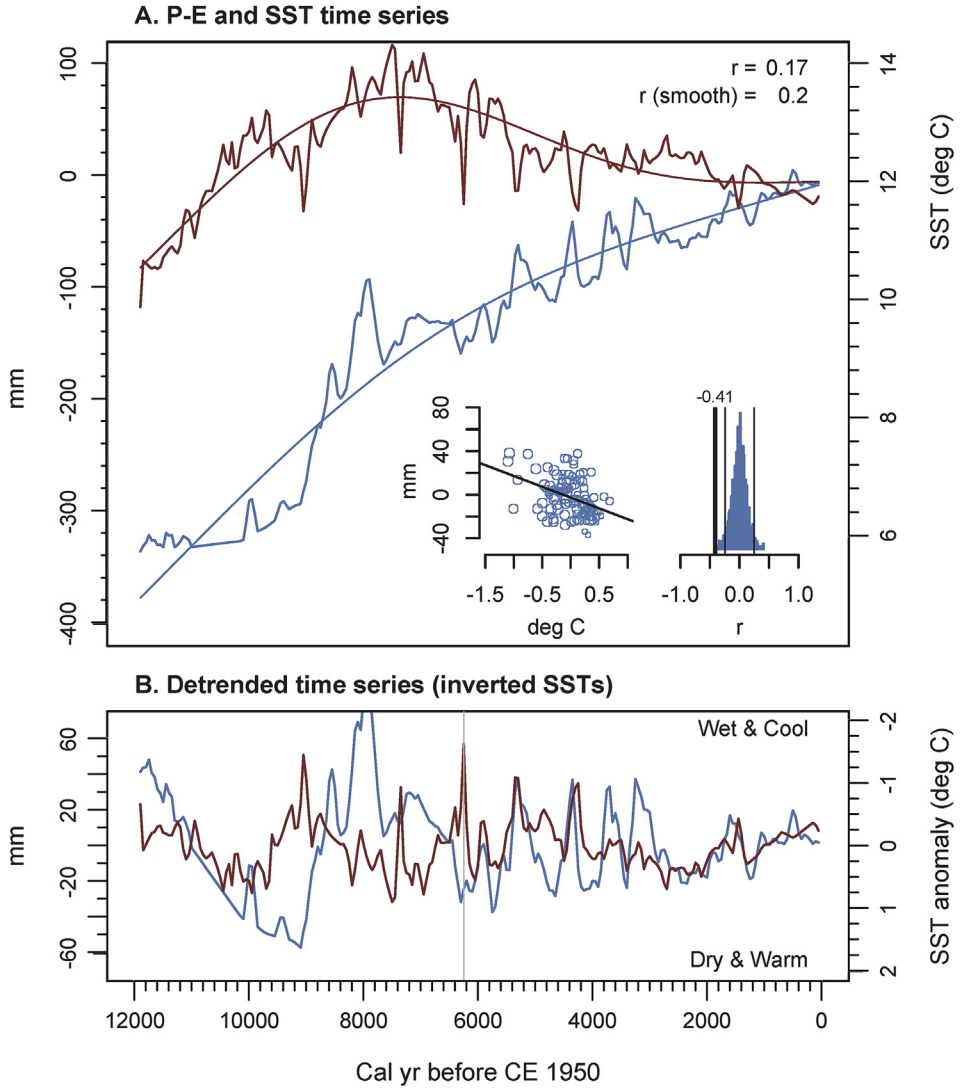

Fig. 3. A) Time series of UK'37 sea-surface temperatures (SST) from OCE327-GCC30 off the Scotian Margin (red, Sachs, 2007; linearly detrended as in Shuman and Marsicek, 2016) and an ensemble of lake-level derived precipitation minus evaporation (P-E) reconstructions (blue, Newby et al., 2014; Shuman and Marsicek, 2016). Bold lines show long-term trends fit using generalized additive mixed models (GAMMs) that account for temporal autocorrelation in the residuals. The inset histogram shows the density of correlation coefficients derived from random, autoregressive time series; thin vertical lines denote the 95% range of values and the bold line indicates the observed correlation in the detrended SST and P-E records (GAMM residuals, shown in B). The inset scatter plot shows the relationship between the detrended SST and P-E records since 6.25 cal kyr BP (left of the thin vertical line in D). For Figs. 3–5, the r values shown at the top right of part A refer to the time series shown in part A, while the bold vertical lines and numbers listed in associated histograms represent the r values for parts B (the detrended series). The scatter plots also show the correlations based on the time series in part B. (For interpretation of the references to colour in this figure legend, the reader is referred to the web version of this article.)

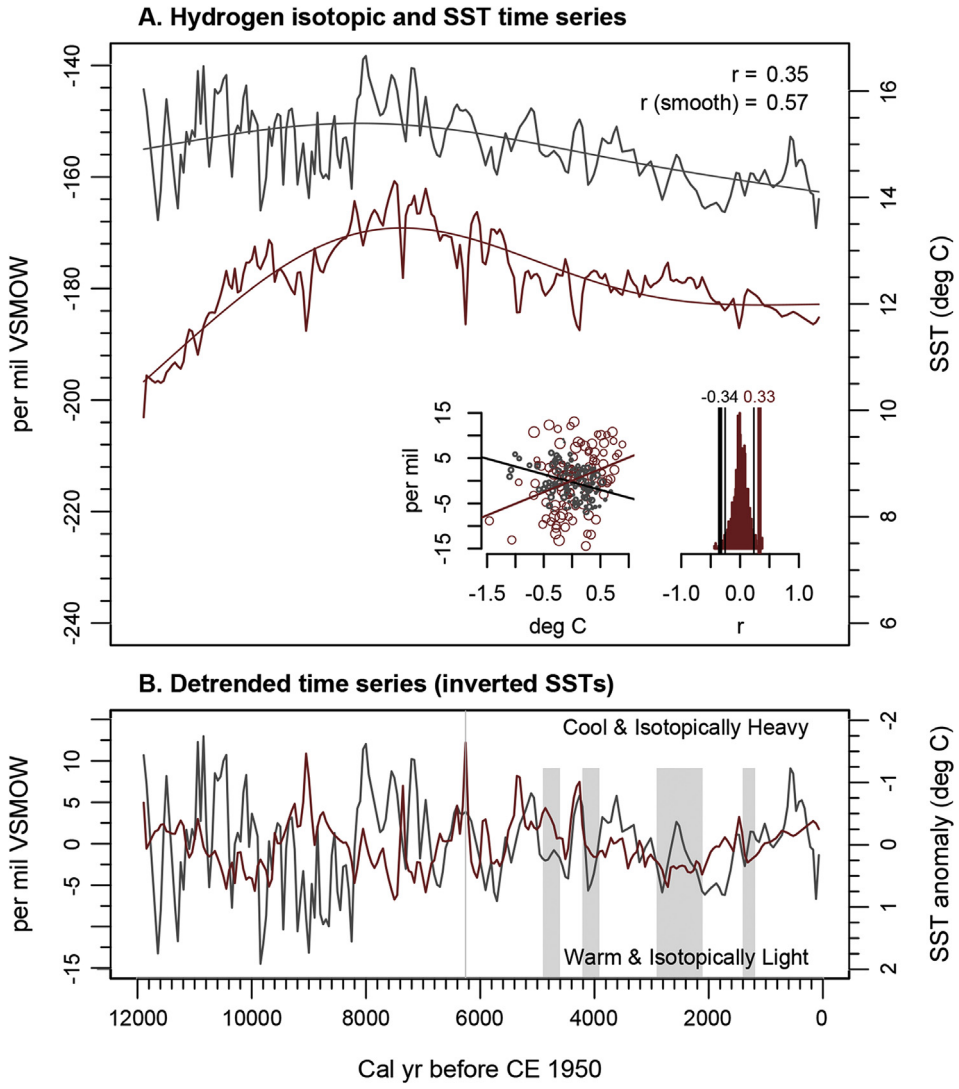

Fig. 4. Same as in Fig. 3 except for the δD_{BA} from Little Pond (black) versus the UK'37 sea-surface temperatures (SST) from OCE327-GCC30 off the Scotian Margin (red, Sachs, 2007; linearly detrended as in Shuman and Marsicek, 2016). In the inset histogram and scatter plot, the black line and symbols indicate the relationships since 6.25 cal kyr BP (left of the thin vertical line in D), whereas the red line and symbols indicate the relationship before 6.25 cal kyr BP. (For interpretation of the references to colour in this figure legend, the reader is referred to the web version of this article.)

relationship ($F > 246$, $p < 2.2e\text{-}16$). Indeed, consistent with the weak correlation between the GAMMs of the SST and P-E series (adjusted $R^2 = 0.03$, $p = 0.002$), the long trend in δD_{BA} appears to be a function of (or related to) independent trends in both temperature and effective moisture: $\delta D_{BA\text{-}smooth} = (3.97 \pm 0.07‰/°C)\ T_{smooth} + (-0.029 \pm 0.0004‰/mm)\ P\text{-}E_{smooth} - 0.02 \pm 0.86‰$ (adjusted $R^2 = 0.96$, $p < 2.2e\text{-}16$).

The residuals of the GAMMs consistently capture a similar series of multi-century events (Figs. 3B–5B), although the correlations related to temperature differ before and after 6.25 cal kyr BP (Fig. 4B). Because the correlations differ significantly from random expectations (Figs. 4A and 5A, inset histograms), the comparisons confirm the presence of a significant signal of multi-century variability that contrasts warm, dry, but isotopically-light phases with cool, wet, and isotopically-heavy phases since 6.25 cal kyr BP (Figs. 4B and 5B).

The correlation of the detrended δD_{BA} and SST series (Fig. 4B, inset scatter plot) has a coefficient near zero and is not significantly different from random correlations when the whole record is considered. However, the lack of correlation arises from two contrasting but significantly different than random correlations before (red in the inset scatter plot, Fig. 4A) and after 6.25 cal kyr BP (gray in the scatter plot). The early-Holocene correlation is positive ($r = 0.33$), but the late-Holocene correlation is negative ($r = -0.34$). The temperature effects on the trends and multi-century events in δD_{BA} over the past 6250 years also reach near equal magnitudes, but have opposite signs. During the multi-century events of the last 6.25 kyr, cool phases coincided with enrichment of deuterium (high δD_{BA} values in the right half, Fig. 4B) rather than the depletion typical of cool precipitation (Dansgaard, 1964) and found in modern surface sediments from northern lakes (Hou et al., 2007): $\delta D_{BA\text{-}detrended} = (-3.4 \pm 0.9‰/°C)\ T_{detrended} - 0.29 \pm 0.29‰$ (adjusted $R^2 = 0.11$, $p = 0.0001$). Granger causality is not detected, however, in the detrended record of multi-century variability ($F < 2.2$, $p > 0.13$).

The comparison of the detrended δD_{BA} and P-E series, however, shows a consistently positive correlation ($r = 0.44$) over the whole record (Fig. 5), which is significantly different from random expectations (inset histogram, Fig. 5A) and exceeds the threshold for Granger causality ($F = 7.5$, $p = 0.007$). Therefore, the relationship

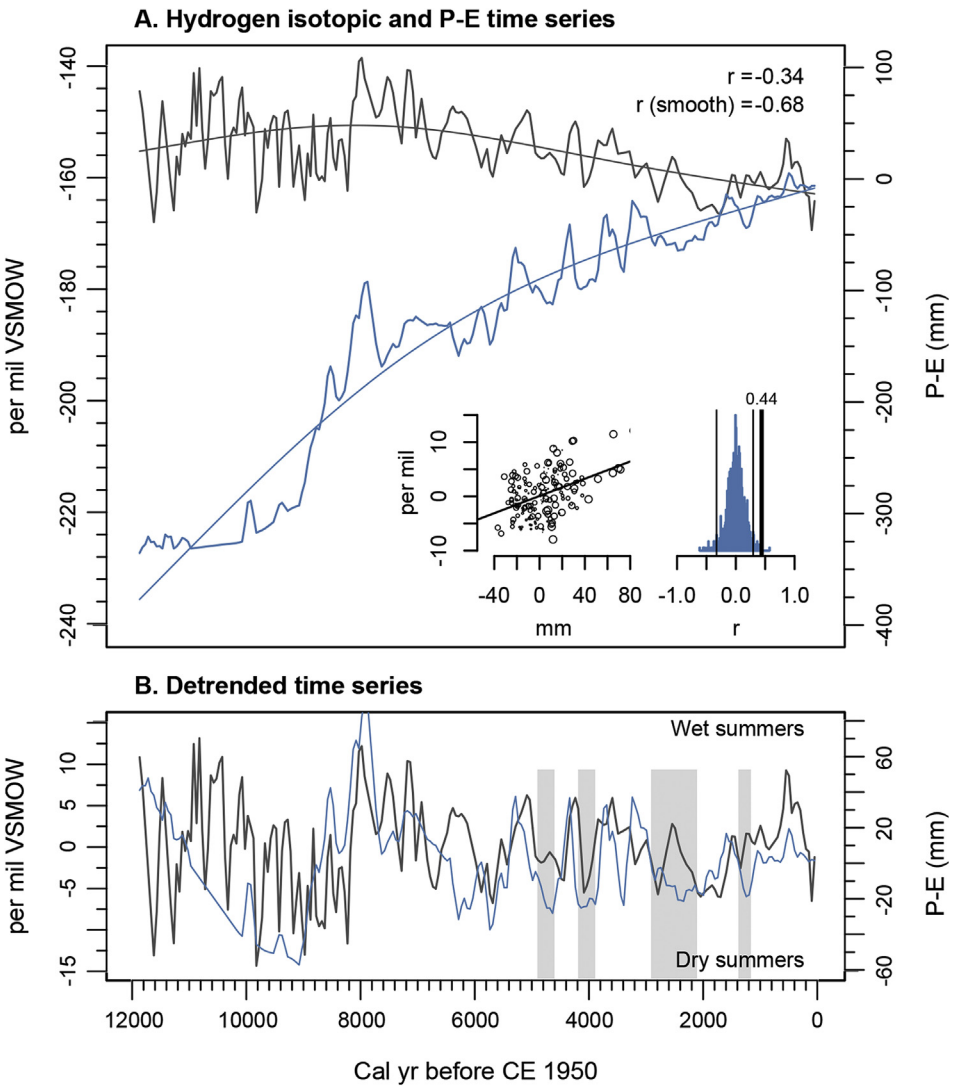

Fig. 5. Same as in Fig. 3 except for the δD_{BA} from Little Pond (black) versus the ensemble of lake-level derived precipitation minus evaporation (P-E) reconstructions (blue, Newby et al., 2014; Shuman and Marsicek, 2016). (For interpretation of the references to colour in this figure legend, the reader is referred to the web version of this article.)

between δD_{BA} and P-E also contrasts depending on frequency: negative correlation with respect to the long trends (Fig. 5A) but positive with respect to the short events (Fig. 5B). Once the long-term trends captured by the GAMMs have been removed, $\delta D_{BA\text{-}detrended}$ = (0.079 ± 0.012‰/mm) $P\text{-}E_{detrended}$ +0.08 ± 0.29‰ (adjusted $R^2 = 0.19$, p = 1.454e-09). Inclusion of temperature into the model reduces the variance explained (adjusted $R^2 = 0.17$, p = 5.255e-06), but overall at the multi-century scale over the past 6250 years, the correlation of warm and dry conditions with reduced enrichment of deuterium with respect to hydrogen contrasts with the expected effects of evaporation on lake water and temperature on precipitation.

3.2. A composite 16ka δD_{BA} record

The composite record of δD_{BA} from Blood and Little Ponds shows significant variations in the hydrogen isotopic values of surface waters in central Massachusetts over the past 16 thousand years (Fig. 6). The composite isotope data after ice volume corrected were shown in Fig. S4. The most prominent temperature change during this period marks the Younger Dryas (YD), which has been extensively discussed in Hou et al. (2007). The total range of the Holocene mean δD_{BA} variation is ~25‰ (based on 5-point running average), which equals only half of the full range from the YD to the Holocene Thermal Maximum based on our scaling of the variance at Blood and Little Ponds.

4. Discussion

4.1. Controls on δD_{BA}

Previous studies have shown that δD values of behenic acid (δD_{BA}) in lake surface sediments of a north-south transect in the eastern United States are strongly correlated to the annual mean air temperature (MAT, in °C), with a transfer function of $\delta D_{BA} = 4.3\ T - 208.4$ ($R^2 = 0.96$) (Hou et al., 2007). The relationship arises from the large spatial scope of the transect, and the first-order correlation of temperature to the δD of precipitation at this scale (Dansgaard, 1964; Rozanski et al., 1993). For similar reasons, we may expect to see a correlation with temperature over time, although the Holocene range of temperatures (~2–4 °C) at any one location is much smaller than the range of temperatures across the

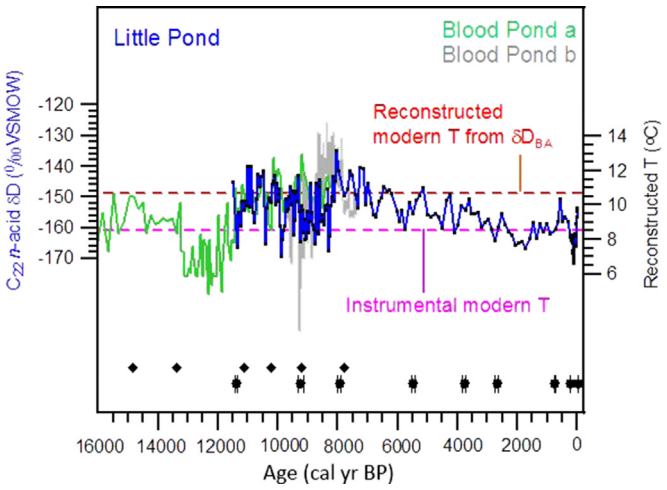

Fig. 6. The composite δD_{BA} record from combining the data of Little Pond (this study) and Blood Pond (Hou et al., 2007; Blood Pond δD values are reduced by 5‰); In (A), the red dashed line marks reconstructed modern temperature using δD_{BA} measured from core top sediment and the pink dashed line marks instrumental modern temperature from the nearby city of Amherst, Massachusetts. Black symbols near bottom of the plots show ^{14}C age controls for the two lake sediment cores (filled diamonds, Blood Pond; filled circles with vertical lines, Little Pond). (For interpretation of the references to colour in this figure legend, the reader is referred to the web version of this article.)

eastern United States (21 °C) (see Hou et al., 2007; Shuman and Marsicek, 2016). The Holocene changes fall within the range of uncertainty in the δD_{BA}-temperature transfer function (Hou et al., 2007): when rearranged, $T = (0.23 \pm 0.02\ °C/‰)\ \delta D_{BA} + 49.0 \pm 2.7\ °C$.

We compared the dDBA-reconstructed temperature with the instrumental record at Amherst, Massachusetts (Fig. 2B). The reconstructed temperatures show similar trends as instrumental annual mean data, but the isotope inferred record was systematically approximately 3 °C warmer than the Amherst record. The discrepancy may arise from several factors. First, leaf wax inferred temperatures are slightly biased toward warmer growth season temperatures for vascular plants in New England. Second, precipitation isotopic ratios can also be affected by many factors such as moisture sources and precipitation seasonality (e.g., Sjostrom and Welker, 2009). In the New England region, seasonal temperature changes play the dominant role in affecting seasonal precipitation isotopic hydrogen ratios (Tang and Feng, 2001; Figs. S5A and S5B), and thus, changes in the proportion of the cold and warm season precipitations can also affect the isotopic ratios of the lake waters (Sjostrom and Welker, 2009). For this reason, δD_{BA} values have been interpreted as precipitation-weighted temperatures rather than annual mean temperature (Hou et al., 2007, 2012), and we expect that the precipitation weighting (as well as other influences) may produce meaningful deviations for mean annual temperature reconstructions over the Holocene (e.g., Shuman and Marsicek, 2016).

We have chosen our study lakes to minimize the potential evaporative effects, but recognize that changes in lake hydrology and morphology over the Holocene may have altered the influence of evaporation through time. Today, the lake waters collected from both Little Pond and Blood Pond plot closely to the local meteoric water line ($\delta D = 7.7\ \delta^{18}O + 8.8$, $R^2 = 0.98$) obtained from GNIP stations in New England (IAEA, 2006), indicating little evaporative enrichment for these flow through lakes with small residence times (Fig. 2A). Our comparisons with other paleoclimate datasets enable us to further evaluate the role of evaporation on δD_{BA} in the past.

We have assessed the aquatic inputs of mid-chain leaf lipids in Little Pond and Blood Pond using the multi-source mixing model developed by Gao et al. (2011). Our results show that above 90% of the total C_{22} *n*-acid in the surface sediments of the two lakes is derived from aquatic floating/submerged macrophytes (Fig. S6, average *n*-alkane distributions for the uppermost 6 sediment samples were displayed for both lakes). Therefore, behenic acid in the two lakes today is contributed predominantly by aquatic plants, minimizing the potential influence from terrestrial plants (Gao et al., 2011). Aquatic floating and submerged plants do not differ significantly in the δD values of their behenic acid (Gao et al., 2011). The dominance of aquatic input may change over time, and may influence the response of leaf lipid δD to P-E conditions to some extent.

4.2. Long-term patterns and relationships

The comparisons with the SST and P-E records from the northeast U.S. (Figs. 3–5) confirm that the Little Pond δD_{BA} record captures multiple climatic signals representative of the region. The isotopic record is particularly important for confirming the presence of a series of multi-century fluctuations since the mid-Holocene as well as a climatic shift at ca. 8.2 ka, which marks the onset of the Holocene Thermal Maximum and an increase in effective moisture (Figs. 4–5). Because the isotopic relationship to climate variables differs, however, between the long-term trends and multi-century events, different climate processes must have been involved. Differences also exist between the climate-driven isotopic dynamics before and after 7-6 cal kyr BP.

The first-order δD_{BA} trends positively correlate with temperature changes (Fig. 4A), and are also negatively correlated with lake-level changes (Fig. 5A). The correlations both far exceed the covariance of temperatures and effective moisture (Fig. 3A), and could reflect long-term changes in factors, such as the evaporative enrichment of deuterium in the lake water, which would combine temperature and effective moisture effects on δD_{BA}. Given the similar magnitudes of the slopes and intercepts in the temperature-δD_{BA} relationships found at this scale (slope: 3.1; intercept: −193; derived from the δD_{BA} and alkenone SST comparison) and in modern samples collected from Florida to Quebec (slope: 4.3; intercept: −208; Hou et al., 2007), the same first-order processes (temperature and effective moisture) may underlie both patterns (Fig. 4A). The SST-δD_{BA} relationship has a 27% lower slope than the modern temperature-δD_{BA} relationship, but only spans ~3 °C compared to the 21 °C range of the modern samples and is not a significantly different relationship given the low number of samples involved (Hou et al., 2007).

Like the SST and pollen-inferred temperatures for the region, we infer peak warmth at ~8 cal kyr BP, 3 kyr later than the summer insolation maximum during the early Holocene (Figs. 4 and 6). If we apply the modern temperature- δD_{BA} transfer function (Hou et al., 2007) to the Little Pond data, the average temperature between 8 and 11 cal kyr BP would have been ~2 °C lower than that of the Holocene Thermal Maximum (HTM) at 7–8 cal kyr BP, which is similar to that inferred from other data sources (Fig. 6; Shuman and Marsicek, 2016). Following the previous interpretations, we attribute this delay relative to summer insolation maximum to the influence of the LIS on the regional climate (Kaufman et al., 2004; Shuman and Marsicek, 2016; Renssen et al., 2009).

Part of the depressed δD_{BA} values from 11 to 8 cal kyr BP, and the rapid positive shift in δD_{BA} at ca. 8.2 ka, may also derive from changes in precipitation seasonality. Previous records suggest that lake levels were low during the early Holocene because the LIS and associated glacial anti-cyclone prevented northward advection of moisture into the region and thus low summer precipitation (Shuman and Donnelly, 2006). The low δD_{BA} values are not consistent with enhanced evaporation from the lakes when water

levels were low, although the specific water level histories of Little and Blood Ponds is not known.

The temperatures inferred from the Little Pond δD_{BA} also display an overall declining trend following the HTM at ~7 cal kyr BP (Fig. 6). The long-term cooling trend of ~3.4 °C, or 0.65°C/kyr between 8 and 2 cal kyr BP corresponds well with declining summer insolation and globally-synthesized borehole temperature (Laskar et al., 2004; Huang et al., 2008). In comparison, the Agassiz and Renland ice cores show ~2.1 °C cooling, whereas pollen-inferred temperatures and the smoothed SST record indicate cooling of up to 2 °C (Sachs, 2007; Vinther et al., 2009; Shuman and Marsicek, 2016). Our results further underscore the likely warm bias in the raw SST reconstructions in the late Pleistocene and early Holocene (Shuman and Marsicek, 2016), especially given that coastal ocean water may have also influenced the air temperature in the northeastern US due to ocean-atmospheric exchange (Shearman and Lentz, 2009). If the δD_{BA} variation is enhanced due to either evaporative effects or a reduced summer:winter precipitation ratio through the Holocene, the inferred temperature change would be even smaller than inferred from the raw (not detrended) SST record (Sachs, 2007).

4.3. Multi-century patterns and relationships

The relationships at the multi-century scale indicate that additional processes have also influenced the record. The correspondence of warm, dry phases with low δD_{BA} values, and cool, wet phases with high δD_{BA} values (Figs. 4B and 5B), is not consistent with either temperature effects on precipitation or evaporative effects on the lake water. Instead, the relationships indicate that the source, atmospheric pathway, or seasonality of moisture (e.g., wet versus dry summers, Fig. 5B) differed between the dynamics that shaped these variables over the long term and during multi-century phases. A key to diagnosing the dynamics undoubtedly also lies in the consistently positive relationship of the detrended δD_{BA} and P-E series (Fig. 5B), whereas the relationships of both these variables with temperature changes at about 6.25 cal kyr BP (Figs. 3B and 4B). Although the long trends were largely driven by orbital and ice sheet changes (Shuman and Marsicek, 2016), a different set of ocean-atmosphere dynamics, perhaps those typical of short-term summer droughts, must be involved in the multi-century variability since 6.25 cal kyr BP.

The multi-century variability in the late-Holocene portion of the δD_{BA} record confirms the warm/dry events at 4.9–4.6, 4.2–3.9, 2.9–2.1, and 1.3–1.2 cal kyr BP, which also altered lake levels (Newby et al., 2014), pollen assemblages (Marsicek et al., 2013), and the Uk'37 temperatures (Sachs, 2007; Shuman and Marsicek, 2016). Given the relationships with temperature and effective moisture (Figs. 4B and 5B), the events either have distinctive atmospheric circulation patterns or represent important changes in the seasonality of precipitation. One parsimonious explanation is that the events represent summer droughts that reduced the ratio of summer over winter precipitation and thus δD_{BA}. The causes, therefore, contrast with the cause of aridity of >300 mm in the early Holocene, which coincides with the opposite direction δD_{BA} change. However, the long-term trend is readily explained by the effects of the Laurentide ice sheet and insolation (e.g., Shuman et al., 2002), whereas additional intrinsic ocean or atmosphere variability that causes multi-century variability could have generated superimposed summer drought events throughout the Holocene – and thus established a consistent relationship between P-E and the detrended δD_{BA} record (Fig. 5B).

Notably, there seems a turning point regarding the detrended PE, δD and SST records at the time scale of centennial to millennial. Before 6.5ka, δD positively correlates to SST at millennial time scale, while PE doesn't seem to exert a prominent control on δD (probably due to the mismatching time intervals between peaks). After 6.5ka, the correlation between δD and SST turns to be negative, while PE shows quite strong and consistent positive control on δD. We introduce the interpretation of wet and dry summer to explain the prominent PE control on δD after 6ka. Briefly, wet summer contributes to heavier δD in precipitation, while SST from coastal N. Atlantic is still annual average.

Two important mechanisms should be considered. First, long-term secular trends in Holocene climates (e.g., driven by insolation change or the permanent loss of the remnant Laurentide Ice Sheet by ca. 6 ka) could have shifted the patterns of atmospheric circulation over the region and thus the teleconnections among regions and the relationships in the data. For example, a gradual shift in the regional influence of the Atlantic subtropical high may have caused the site to cross from one side to another of key frontal boundaries (e.g., the seasonal Arctic front). The result would be a local state-shift in climate-isotopic relationships arising from a gradual regional change. Alternatively, the change could represent a shift in the dynamics of the North Atlantic. Reconstructions of North Atlantic overturning (e.g., Thornalley et al., 2009) reveal a mid-Holocene shift from a stable overturning state before ca. 6 ka to repeated multi-century variability during the late-Holocene.

4.4. The composite 16ka δD_{BA} record

We use the composite to highlight that although cooling during the YD produced a significant negative excursion in δD_{BA}, such a strong positive correlation with temperature does not extend into the late-Holocene at similar multi-century scales – at least at Little Pond (Fig. 4B). The comparison with the SST reconstruction (Fig. 4) indicates that a positive relationship between δD_{BA} and SSTs extends until ~7 cal kyr BP (red symbol, inset scatter plot in Fig. 4A; left half, Fig. 4B), but more fine variability exists within the two δD_{BA} records than the SST record. Similar to Blood Pond, Little Pond records multiple large centennial-scale δD excursions between 11.3 and 8 cal kyr BP with similar magnitude to that of the 8.2 ka event (Fig. 6). These multi-decadal to multi-centennial negative excursions in the Little Pond δD_{BA} record are roughly centered at 10.7, 10.2, 9.8, 9.4, 9.2, 8.9, 8.5 and 8.2 cal kyr BP, within the uncertainty of the age model for the Little Pond, and likely have climatic significance given the significant agreement of late-Holocene events across different types of records (Figs. 3–5).

We cannot statistically compare these with equally-detailed quantitative moisture records from the region (Fig. 5), but the events are broadly consistent with detailed drought history derived from coarse material proportions in the high-sedimentation, nearshore record from Rocky Pond, Massachusetts, indicating regional responses to common climate forcings (Fig. 4; Newby et al., 2009). The negative isotopic excursions at sub-millennial scales are not, however, consistent with evaporative enrichment during the drought episodes. Instead, they likely extend the moisture-isotope relationship that we found since 8.5 cal kyr BP through our comparison with the regional P-E reconstruction (Fig. 5B).

5. Conclusions

In this study, we present a high-resolution record of hydrogen isotope ratios of behenic acid (δD_{BA}) from Little Pond and Blood Pond in Massachusetts, USA. The record contains multiple signals at multi-millennial to multi-century scales that significantly correlate with temperature and effective moisture reconstructions from the region. Importantly, however, the signs of these relationships differ both across scales and between the early and late portions of the record. In this way, the data help to diagnose the spectrum of

different climate dynamics involved in the region. Our data indicate a Holocene Thermal Maximum between 8 and 7 cal kyr BP, which is ~2 °C warmer than the average of early Holocene temperatures in the study region. The inference is consistent with both a modern temperature-δD_{BA} transfer function, and the long-term correlation between the δD_{BA} record and alkenone-derived SSTs. We attribute the lower regional temperature in the early Holocene to the LIS, which may suppress the movement of subtropical air mass northward. Our Little Pond record also replicates abrupt cooling events revealed in Blood Pond δD_{BA} record, and confirms the existence of a prominent multi-century variability including a rapid shift at ca. 8.2 ka and at 4.9–4.6, 4.2–3.9, 2.9–2.1, and 1.3–1.2 cal kyr BP. The later have a different relationship to temperature than inferred over the long term, which appears to be a function of dynamics that generated summer drought across the region.

Acknowledgements

Grants NSF 0318050, 0816739, 0902805 and 1024144 to Y. Huang and Grant NSF DEB-0815036 to D. Foster, B. Shuman, Y. Huang and W. Oswald, supported this research. We thank Dr. James Russell, Dr. Bette Otto-Bliesner and Dr. Warren Prell for valuable discussions. We thank Prof. Colin V. Murray-Wallace, Dr. Hillaire-Marcel and two anonymous reviewers for the constructive comments to improve this manuscript.

Appendix A. Supplementary data

Supplementary data related to this article can be found at http://dx.doi.org/10.1016/j.quaint.2017.06.053.

References

Bradley, R.S., Eischeid, J.K., Ives, P.T., 1987. The Climate of Amherst, Massachusetts. Department of Geology and Geography, University of Massachusetts, Amherst, Amherst College, pp. 1836–1985. Contribution No. 50. http://www.geo.umass.edu/research/Geosciences%20Publications/v50BradleyetalCovered.pdf.

Cwynar, L.C., Spear, R.W., 2001. Lateglacial climate change in the white mountains of New Hampshire. Quat. Sci. Rev. 20, 1265–1274.

Dansgaard, W., 1964. Stable isotopes in precipitation. Tellus 16, 436–468.

Francis, D.R., Foster, D.R., 2001. Response of small New England ponds to historic land use. Holocene 11, 301–312.

Gao, L., Hou, J., Toney, J., MacDonald, D., Huang, Y., 2011. Mathematical modeling of the aquatic macrophyte inputs of mid-chain *n*-alkyl lipids to lake sediments: implications for interpreting compound specific hydrogen isotopic records. Geochim. Cosmochim. Acta 75, 3781–3791.

Gao, L., Burnier, A., Huang, Y., 2012. Quantifying instantaneous regeneration rates of plant leaf waxes using stable hydrogen isotope labeling. Rapid Commun. Mass Spectrom. 26, 115–122.

Grootes, P.M., Stuiver, M., 1997. Oxygen 18/16 variability in Greenland snow and ice with 10^3– to 10^5- year time resolution. J. Geophys. Res. 102, 26455–26470.

Haslett, J., Parnell, A., 2008. A simple monotone process with application to radiocarbon-dated depth chronologies. J. R. Stat. Soc. Ser. C.

Hou, J., Huang, Y., Wang, Y., Shuman, B., Oswald, W.W., Faison, E., Foster, D.R., 2006. Postglacial climate reconstruction based on compound-specific D/H ratios of fatty acids from blood pond, New England. Geochem. Geophys. Geosys. 7, Q03008.

Hou, J., Huang, Y., Oswald, W.W., Foster, D.R., Shuman, B., 2007. Centennial-scale compound-specific hydrogen isotope record of Pleistocene-Holocene climate transition from southern New England. Geophys. Res. Lett. 34.

Hou, J., Huang, Y., Shuman, B.N., Oswald, W.W., Foster, D.R., 2012. Abrupt cooling repeatedly punctuated early-Holocene climate in eastern North America. Holocene 22, 525–529.

Huang, S.P., Pollack, H.N., Shen, P.Y., 2008. A late Quaternary climate reconstruction based on borehole heat flux data, borehole temperature data, and the instrumental record. Geophys. Res. Lett. 35, L13703.

Huang, Y., Shuman, B., Wang, Y., Webb III, T., 2002. Hydrogen isotope ratios of palmitic acid in lacustrine sediments record late Quaternary climate variations. Geology 30, 1103–1106.

Huang, Y., Shuman, B., Wang, Y., Webb III, T., 2004. Hydrogen isotope ratios of individual lipids in lake sediments as novel tracers of climatic and environmental change: a surface sediment test. J. Paleolimnol. 31, 363–375.

Hubeny, J.B., King, J.W., Reddin, M., 2011. Northeast US precipitation variability and North American climate teleconnections interpreted from late Holocene varved sediments. Proc. Natl. Acad. Sci. 108, 17895–17900.

IAEA, 2006. Isotope Hydrology Information System. The isohis database. Accessible at: http://www.Iaea.Org/water.

Kaufman, D.S., Ager, T.A., Anderson, N.J., Anderson, P.M., Andrews, J.T., Bartlein, P.J., Brubaker, L.B., Coats, L.L., Cwynar, L.C., Duvall, M.L., Dyke, A.S., Edwards, M.E., Eisner, W.R., Gajewski, K., Geirsdóttir, A., Hu, F.S., Jennings, A.E., Kaplan, M.R., Kerwin, M.W., Lozhkin, A.V., MacDonald, G.M., Miller, G.H., Mock, J., Oswald, W.W., Otto-Bliesner, B.L., Porinchu, D.F., Rühland, K., Smol, J.P., Steig, E.J., Wolfe, B.B., 2004. Holocene thermal maximum in the Western Arctic (0-180°w). Quat. Sci. Rev. 23, 529–560.

Laskar, J., Robutel, P., Joutel, F., Gastineau, M., Correia, A.C.M., Levrard, B., 2004. A long-term numerical solution for the insolation quantities of the Earth. Astron. Astrophys. 428, 261–285.

Marsicek, J.P., Shuman, B., Brewer, S., Foster, D.R., Oswald, W.W., 2013. Moisture and temperature changes associated with the mid-Holocene Tsuga decline in the northeastern United States. Quat. Sci. Rev. 80, 129–142. http://dx.doi.org/10.1016/j.quascirev.2013.09.001.

Newby, P.E., Donnelly, J.P., Shuman, B.N., MacDonald, D., 2009. Evidence of centennial-scale drought from southeastern Massachusetts during the Pleistocene/Holocene transition. Quat. Sci. Rev. 28, 1675–1692.

Newby, P., Shuman, B., Donnelly, J.P., Karnauskas, K.B., Marsicek, J.P., 2014. Centennial-to-Millennial hydrologic trends and variability along the north atlantic coast, U.S.A., during the holocene. Geophys. Res. Lett. 41 http://dx.doi.org/10.1002/2014GL060183.

Nichols, J.E., Huang, Y., 2012. Hydroclimate of the northeastern United States is highly sensitive to solar forcing. Geophys. Res. Lett. 39, L04707.

Norton, S.A., Brakke, D.F., Kahf, J.S., Haines, T., 1989. Major influences on lake water chemistry in Maine. Stud. Maine Geol. 5.

Oswald, W.W., Faison, E.K., Foster, D.R., Doughty, E.D., Hall, B.R., Hansen, B.C.S., 2007. Post-glacial changes in spatial patterns of vegetation across southern New England. J. Biogeogr. 34, 900–913.

Oswald, W.W., Foster, D.R., Doughty, E.D., Macdonald, D., 2010. A record of Holocene environmental and ecological changes from wildwood lake, long island, New York. J. Quat. Sci. 25, 967–974.

Puntsag, T., Mitchell, M., Campbell, J., Klein, E.S., Likens, G.E., Welker, J.M., 2016. Arctic Vortex changes alter the sources and isotopic values of precipitation in northeastern US. Sci. Rep. 6, 22647 http://dx.doi.org/10.1038/srep22647.

R Core Development Team, 2009. R: a Language and Environment for Statistical Computing. R Foundation for Statistical Computing, Vienna, Austria.

Renssen, H., Seppa, H., Heiri, O., Roche, D.M., Goosse, H., Fichefet, T., 2009. The spatial and temporal complexity of the Holocene thermal maximum. Nat. Geosci. 2, 411–414.

Rolph, G.D., 2017. Real-time Environmental Applications and Display SYstem (READY) Website. NOAA Air Resources Laboratory, College Park, MD. http://www.ready.noaa.gov.

Rozanski, K., Araguás-Araguás, L., Gonfiantini, R., 1993. Isotopic patterns in modern global precipitation. In: Swart, P.K. (Ed.), Climate Change in Continental Isotopic Records, Geophys. Monogr. Ser., vol. 78. AGU, Washington, D. C, pp. 1–36.

Sachs, J.P., 2007. Cooling of northwest Atlantic slope waters during the Holocene. Geophys. Res. Lett. 34, L03609.

Shearman, R.K., Lentz, S.J., 2009. Long-term sea surface temperature variability along the U.S. East coast. J. Phys. Oceanogr. 40, 1004–1017.

Shuman, B., Donnelly, J.P., 2006. The influence of seasonal precipitation and temperature regimes on lake levels in the northeastern United States during the Holocene. Quat. Res. 65, 44–56.

Shuman, B.N., Marsicek, J.P., 2016. The structure of holocene climate change in mid-latitude north America. Quat. Sci. Rev. 141, 38–51.

Shuman, B., Bravo, J., Kaye, J., Lynch, J.A., Newby, P., Webb III, T., 2001. Late-Quaternary water-level variations and vegetation history at Crooked Pond, southeastern Massachusetts. Quat. Res. 56, 401–410.

Shuman, B., Bartlein, P., Logar, N., Newby, P., Webb III, T., 2002. Parallel climate and vegetation responses to the early-Holocene collapse of the Laurentide Ice Sheet. Quat. Sci. Rev. 21, 1793–1805.

Shuman, B., Huang, Y., Newby, P., Wang, Y., 2006. Compound-specific isotopic analyses track changes in seasonal precipitation regimes in the northeastern United States at ca 8200 cal yr BP. Quat. Sci. Rev. 25, 2992–3002.

Shuman, B., Bartlein, P.J., Webb III, T., 2007. Response to "comments on: 'The magnitude of millennial- and orbital-scale climatic change in eastern North America during the late-Quaternary' by shuman et al." Quat. Sci. Rev. 26, 268–273.

Sjostrom, D., Welker, J.M., 2009. The influence of air mass source on the seasonal isotopic composition of precipitation, eastern USA. J. Geochem. Explor. 102, 103–112.

Stein, A.F., Draxler, R.R., Rolph, G.D., Stunder, B.J.B., Cohen, M.D., Ngan, F., 2015. NOAA's HYSPLIT atmospheric transport and dispersion modeling system. Bull. Am. Meteor. Soc. 96, 2059–2077. http://dx.doi.org/10.1175/BAMS-D-14-00110.1.

Tang, K.L., Feng, X.H., 2001. The effect of soil hydrology on the oxygen and hydrogen isotopic compositions of plants' source water. Earth Planet. Sci. Lett. 185 (3–4), 355–367.

Thornalley, David J.R., Elderfield, Harry, McCave, I. Nick, 2009. Holocene oscillations in temperature and salinity of the surface subpolar North Atlantic. Nature 457, 711–714.

Viau, A.E., Gajewski, K., Sawada, M.C., Fines, P., 2006. Millennial-scale temperature variations in north America during the Holocene. J. Geophys. Res. 111, D09102.

Vinther, B.M., Buchardt, S.L., Clausen, H.B., Dahl-Jensen, D., Johnsen, S.J., Fisher, D.A., Koerner, R.M., Raynaud, D., Lipenkov, V., Andersen, K.K., Blunier, T.,

Rasmussen, S.O., Steffensen, J.P., Svensson, A.M., 2009. Holocene thinning of the Greenland ice sheet. Nature 461, 385–388.
Wang, X., Auler, A.S., Edwards, R.L., Cheng, H., Cristalli, P.S., Smart, P.L., Richards, D.A., Shen, C.C., 2004. Wet periods in northeastern Brazil over the past 210 kyr linked to distant climate anomalies. Nature 432, 740–743.
Wang, Y., Cheng, H., Edwards, R.L., Kong, X., Shao, X., Chen, S., Wu, J., Jiang, X., Wang, X., An, Z., 2008. Millennial- and orbital-scale changes in the East Asian monsoon over the past 224,000 years. Nature 451, 1090–1093.
Webb III, T., Shuman, B., Leduc, P., Newby, P., Miller, N., 2003. Late Quaternary climate history of western New York State. Bull. Buffalo Soc. Nat. Sci. 37, 11–13.
Williams, J.W., Shuman, B., Bartlein, P.J., Diffenbaugh, N.S., Webb III, T., 2010. Rapid, time-transgressive, and variable responses to early Holocene midcontinental drying in North America. Geology 38, 135–138.
Wood, S.N., 2006. Generalized Additive Models: an Introduction with R, Chapman & Hall/CRC Texts in Statistical Science. Chapman and Hall/CRC.